Supporting Information

Amphiphilic core-sheath structured composite fiber for comprehensively performed supercapacitor

Xuemei Fu,[1] Zhuoer Li,[1] Limin Xu,[1] Meng Liao,[1] Hao Sun,[2] Songlin Xie,[1] Xuemei Sun,[1] Bingjie Wang[1,*] and Huisheng Peng[1,*]

[1] Laboratory of Advanced Materials, State Key Laboratory of Molecular Engineering of Polymers and Department of Macromolecular Science, Fudan University, Shanghai 200438, China

[2] Department of Chemistry, Stanford University, Stanford, California 94305, United States

*Corresponding authors (emails: wangbingjie@fudan.edu.cn (Wang B); penghs@fudan.edu.cn (Peng H)).

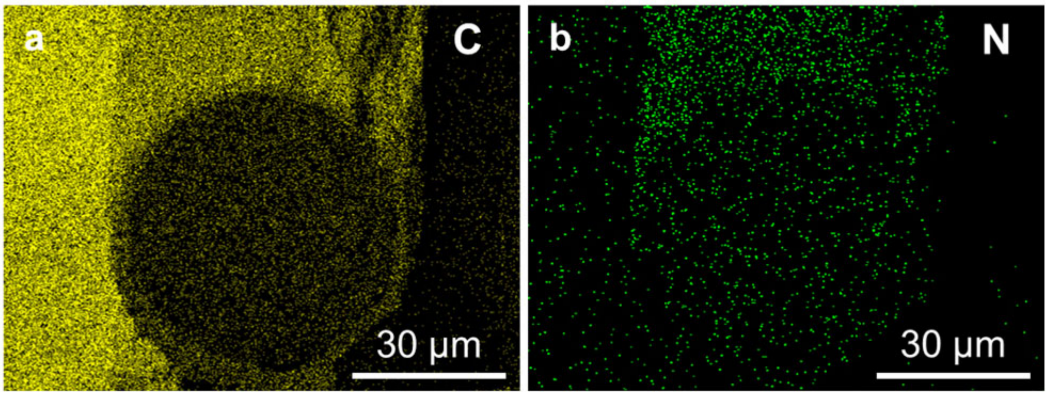

Figure S1 EDS element mapping of (a) C and (b) N elements in **Figure 1**c.

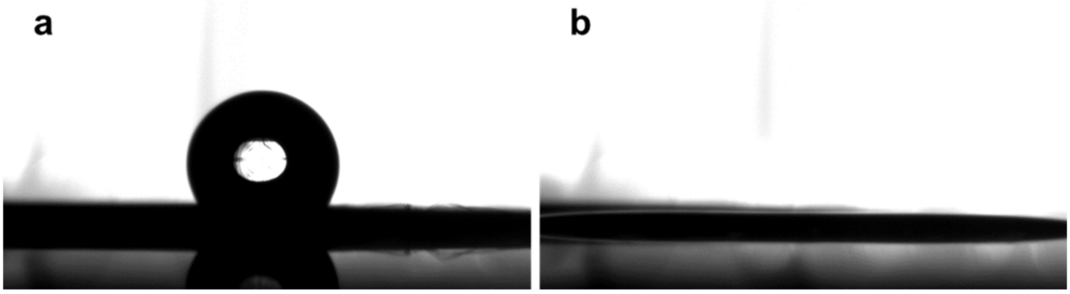

Figure S2 The water contact angle of (a) CNT sheets and (b) OCNT sheets.

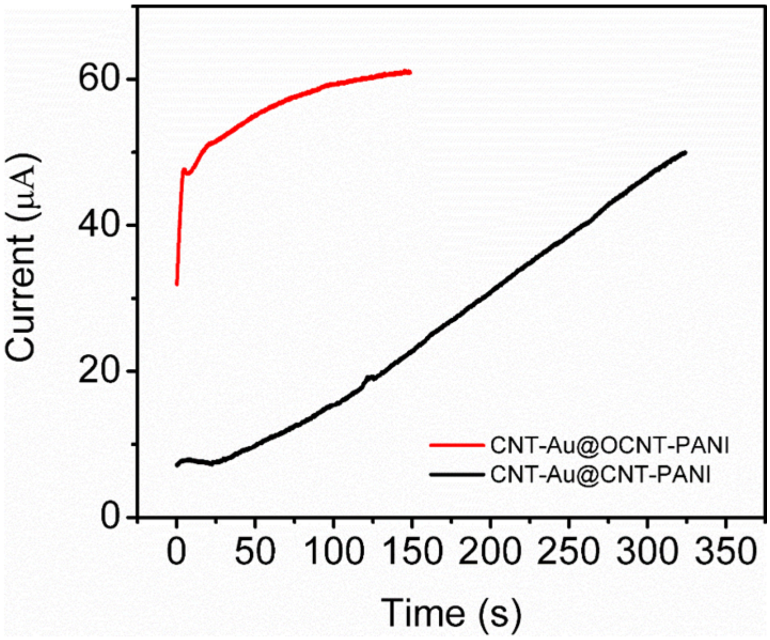

Figure S3 The electrochemical polymerization process of PANI on fibers with hydrophobic CNT and hydrophilic OCNT sheath via a potentiostatic method, respectively. Here the loading of PANI is 30 wt.%.

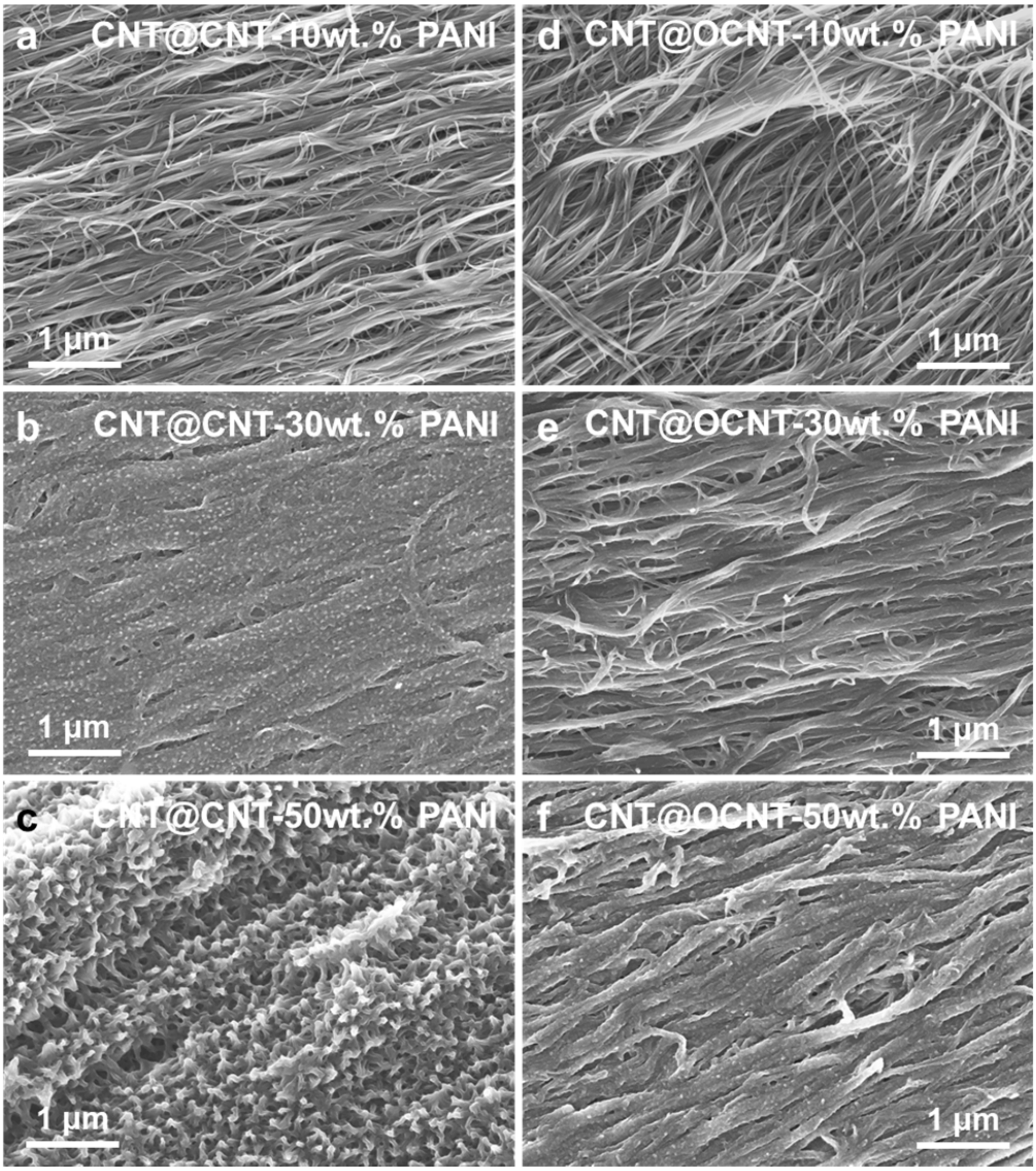

Figure S4 Morphology characterization of (a-c) CNT@CNT-PANI and (d-f) CNT@OCNT-PANI fibers with PANI contents from 10 to 50 wt.%.

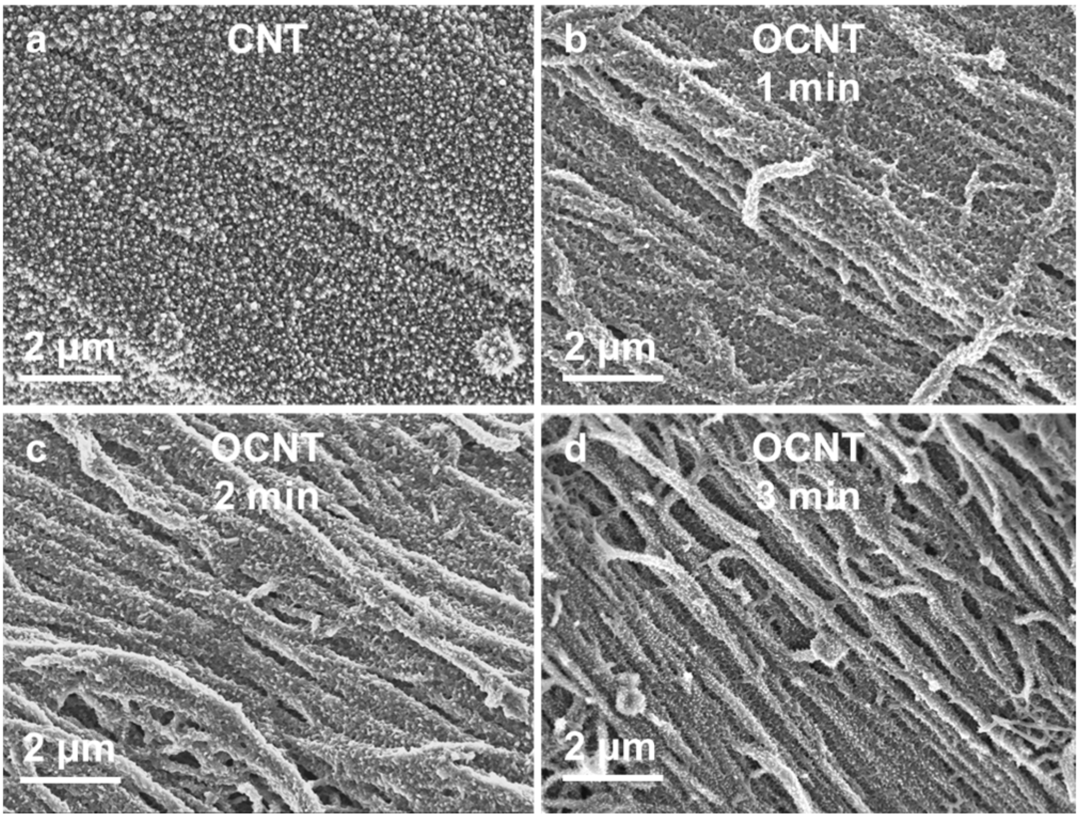

Figure S5 Compared with (a) CNT@CNT-PANI fiber, morphology characterization of CNT@OCNT-PANI fibers at a PANI content of 70 wt.% with OCNT obtained by oxygen plasma treatment for (b) 1 min, (c) 2 min and (d) 3 min.

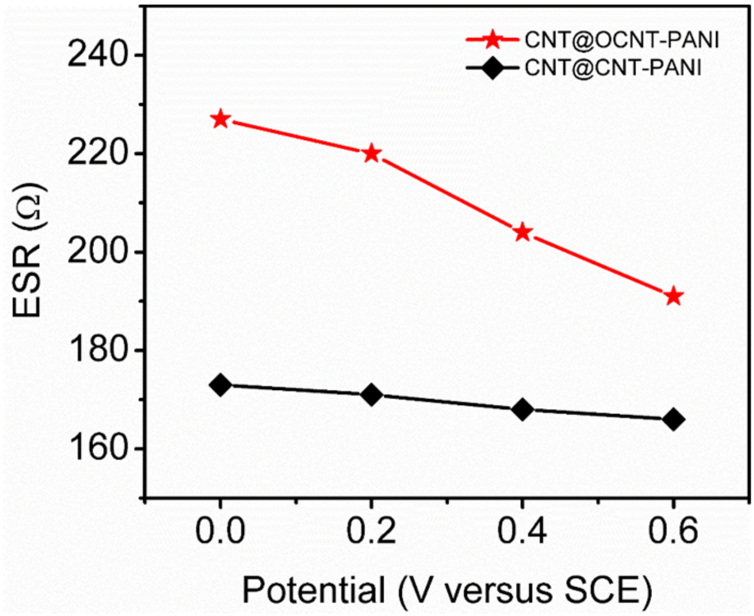

Figure S6 The dependence of ESR on the applied potential for CNT@CNT-PANI and CNT@OCNT-PANI electrodes in a three-electrode system, respectively.

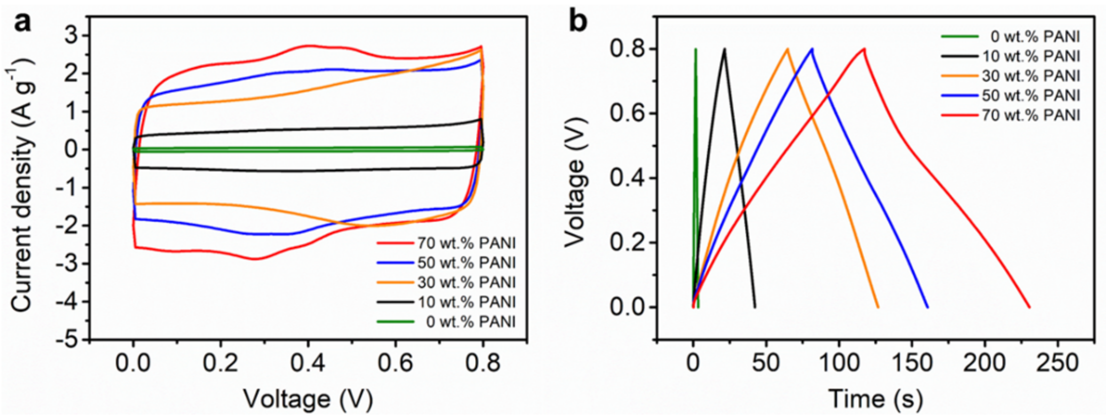

Figure S7 (a) CV measurement at 20 mV s^{-1} and (b) GCD characterization at 1 A g^{-1} for fiber-shaped supercapacitors based on CNT@CNT-PANI with PANI contents from 0 to 70 wt.% in a gel electrolyte.

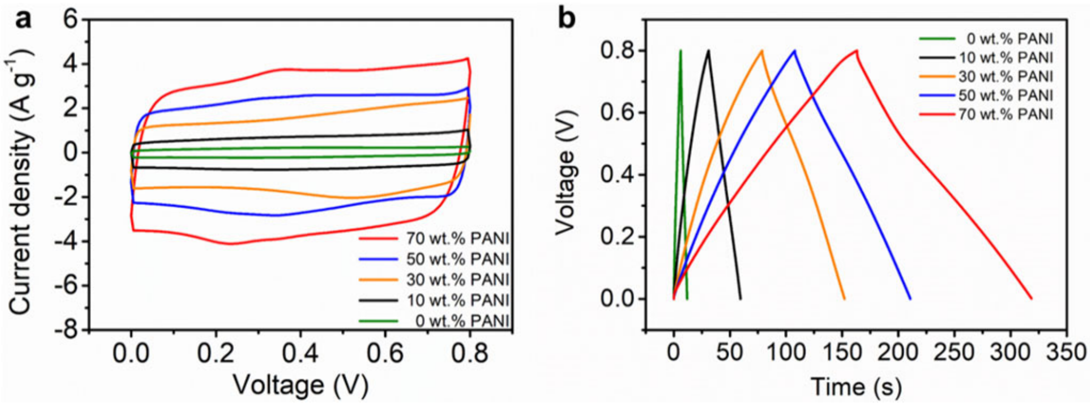

Figure S8 (a) CV measurement at 20 mV s^{-1} and (b) GCD characterization at 1 A g^{-1} for fiber-shaped supercapacitors based on CNT@OCNT-PANI with PANI contents from 0 to 70 wt.% in a gel electrolyte.

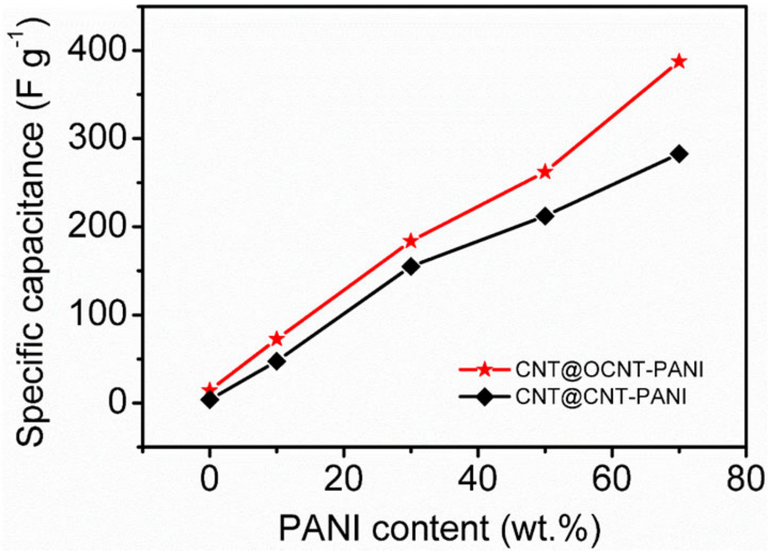

Figure S9 Specific capacitance as a function of PANI content at 1 A g^{-1} for a comparison of CNT@CNT-PANI and CNT@OCNT-PANI fibers.

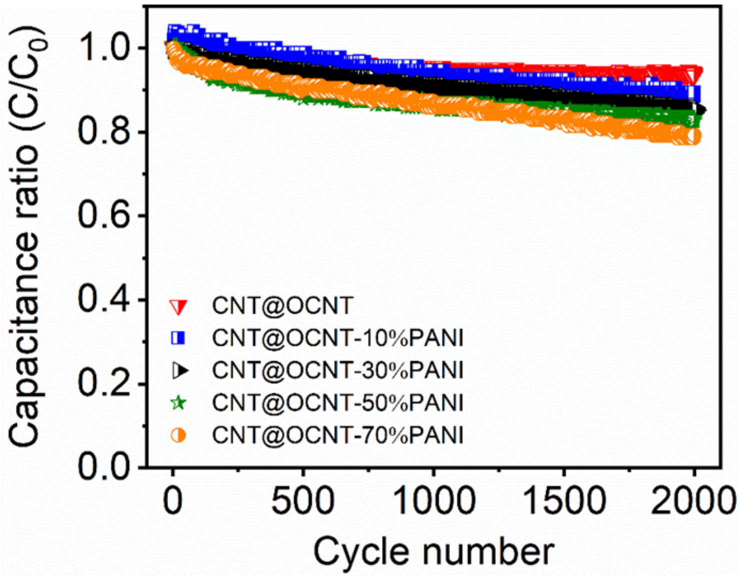

Figure S10 Cycle life comparison of the fiber-shaped supercapacitors with PANI loading from 0 to 70 wt.%. C_0 and C referred to the capacitances before and after cycling, respectively.

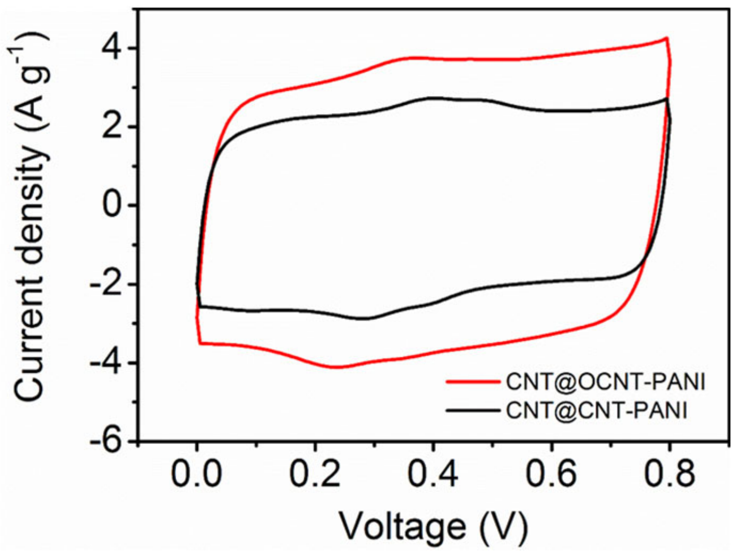

Figure S11 CV curves of supercapacitors based on CNT@OCNT-PANI and CNT@CNT-PANI with 70 wt.% PANI content with gel electrolyte.

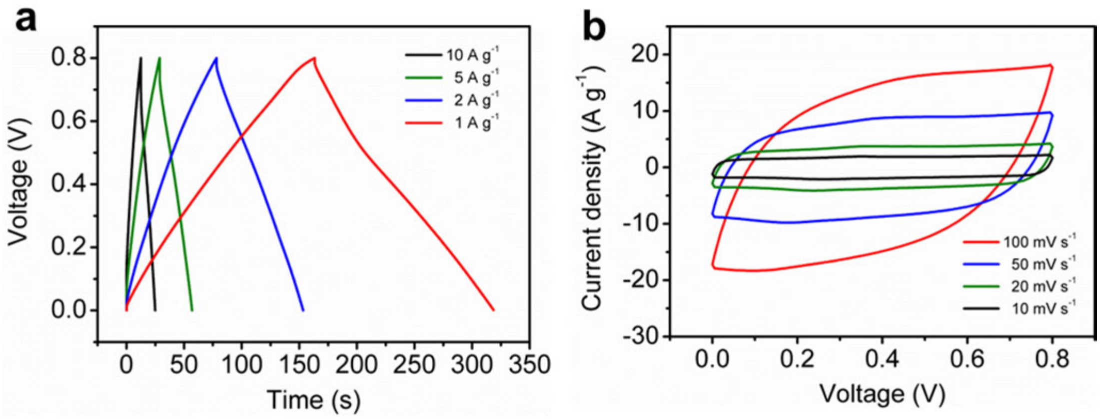

Figure S12 (a) Typical GCD curves at different current densities and (b) CV curves at different scan rates of the supercapacitor using CNT@OCNT-PANI fibers with 70 wt.% PANI content based on gel electrolyte.

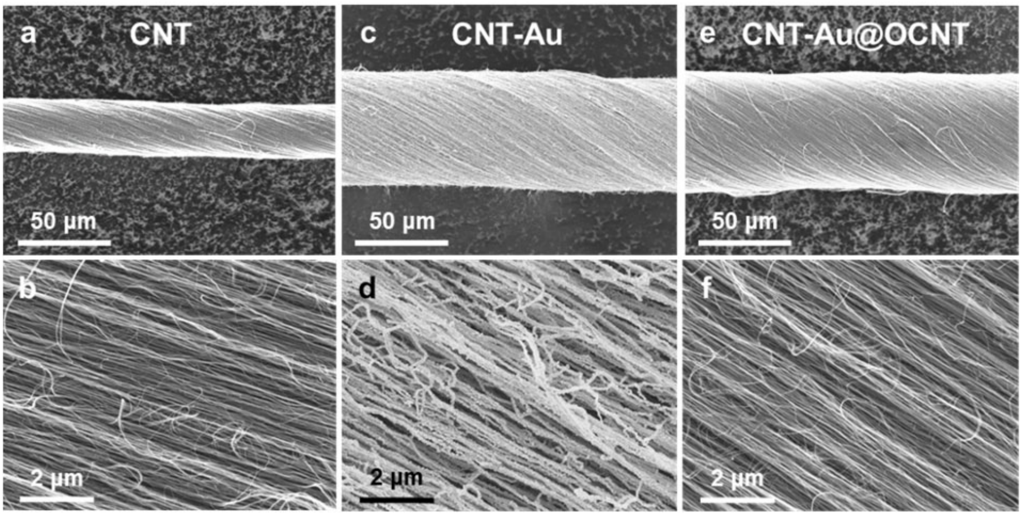

Figure S13 (a, b) SEM images of CNT fiber at low and high magnifications, respectively. (c, d) SEM images of CNT-Au fiber at low and high magnifications, respectively, followed by winding OCNT sheets (e, f).

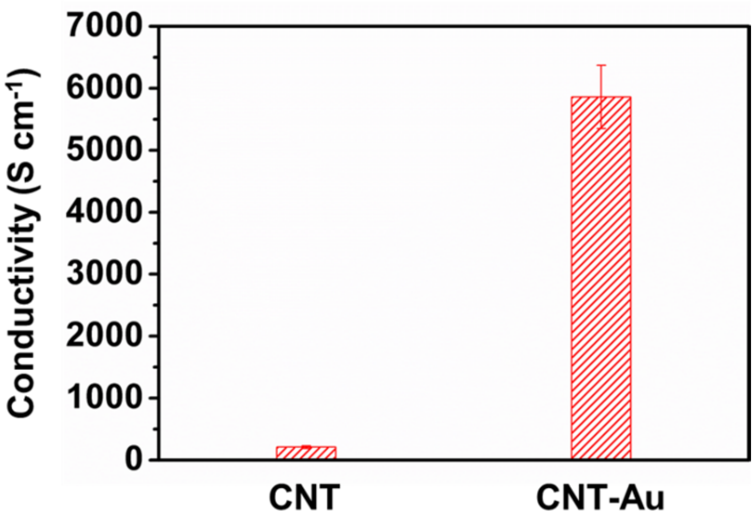

Figure S14 Electrical conductivities of bare CNT fibers and Au-deposited CNT fibers.

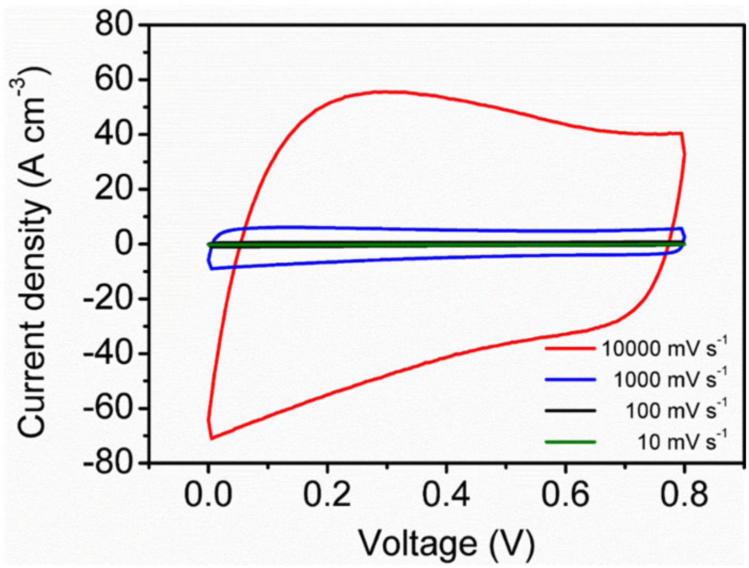

Figure S15 CV characterization at different scan rates of the supercapacitor based on CNT-Au@OCNT fibers with gel electrolyte.

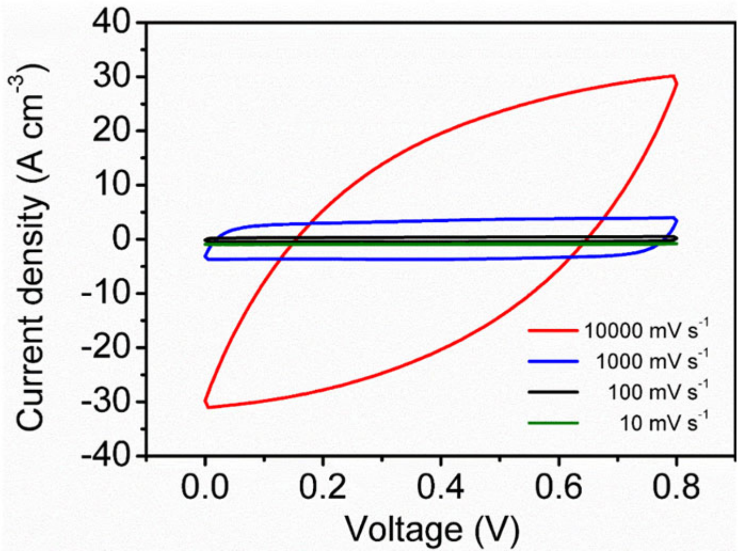

Figure S16 CV characterization at different scan rates of the supercapacitor based on CNT@OCNT fibers with gel electrolyte.

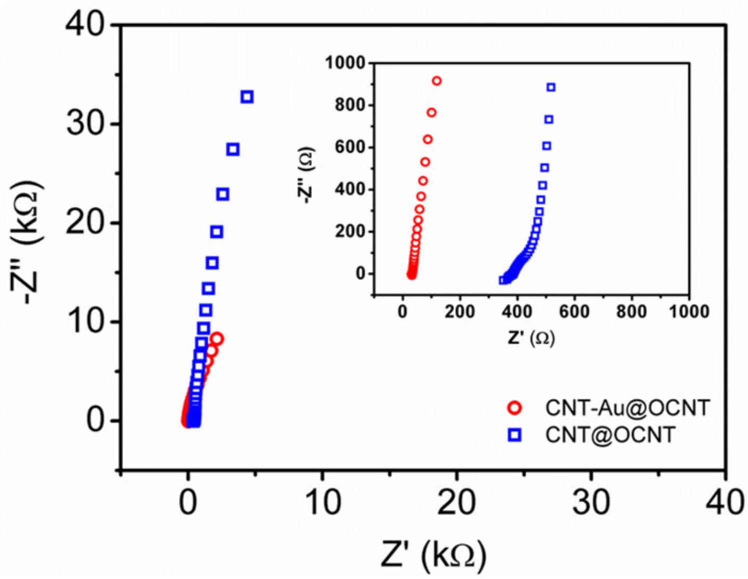

Figure S17 Nyquist plot comparison of fiber-shaped supercapacitors using CNT-Au@OCNT and CNT@OCNT with gel electrolyte. The high frequency region is highlighted in the inserted panel.

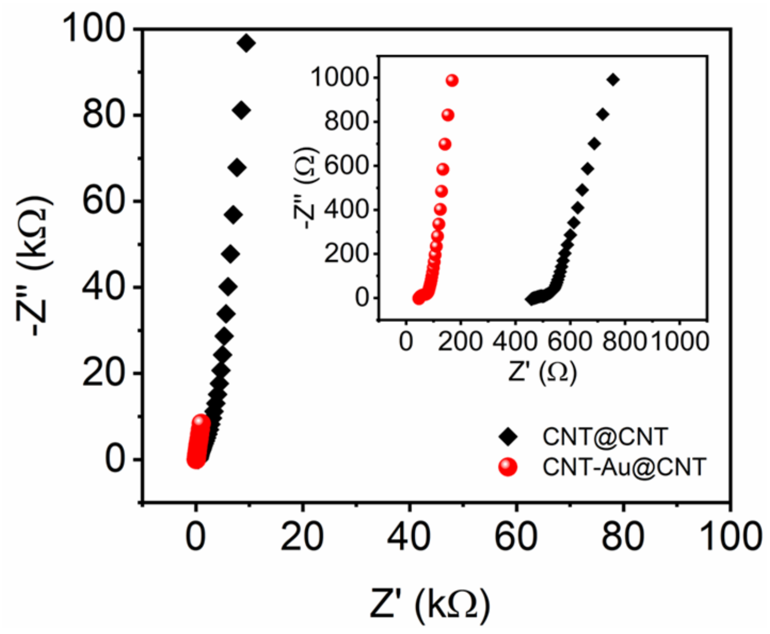

Figure S18 Nyquist plot comparison of fiber-shaped supercapacitors using CNT-Au@CNT and CNT@CNT with gel electrolyte. The high frequency region is highlighted in the inserted panel.

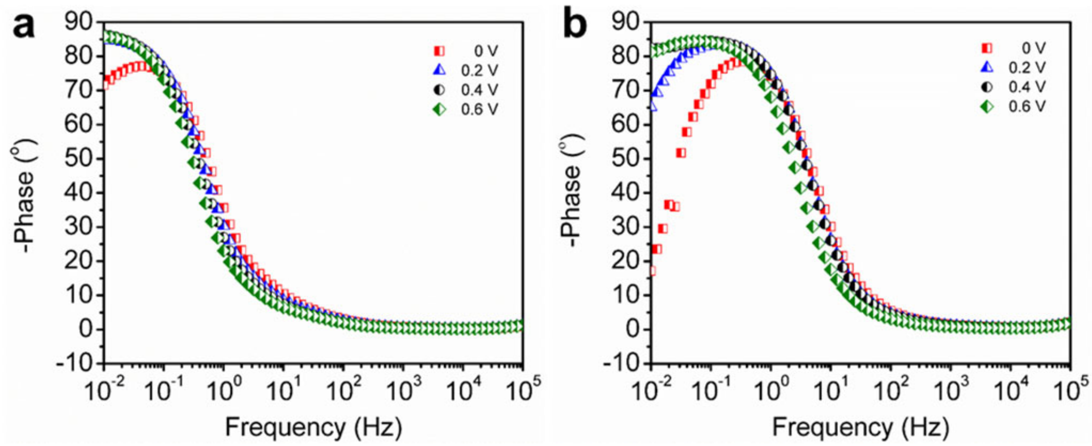

Figure S19 Dependence of impedance phase angle on frequency for (a) CNT@OCNT-PANI and (b) CNT-Au@OCNT-PANI electrodes at different potentials versus SCE.

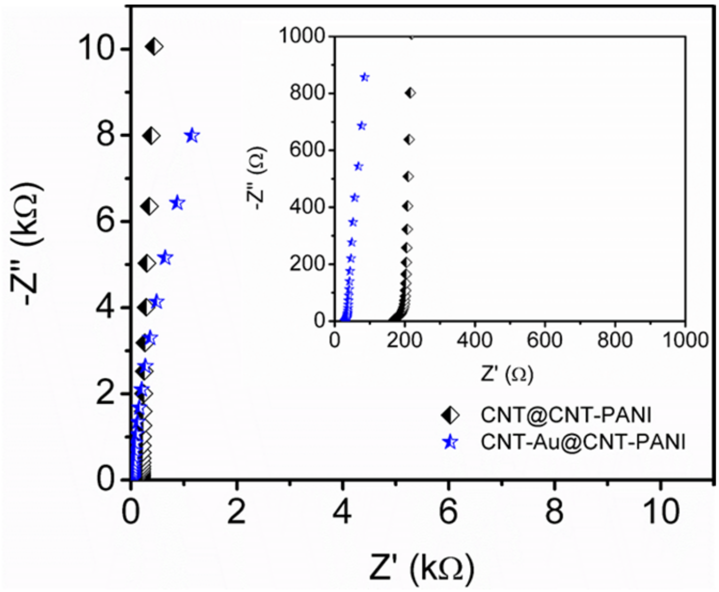

Figure S20 Comparison of Nyquist plots of CNT@CNT-PANI and CNT-Au@CNT-PANI electrodes at 0.6V versus SCE. The high frequency region is highlighted in the inserted panel.

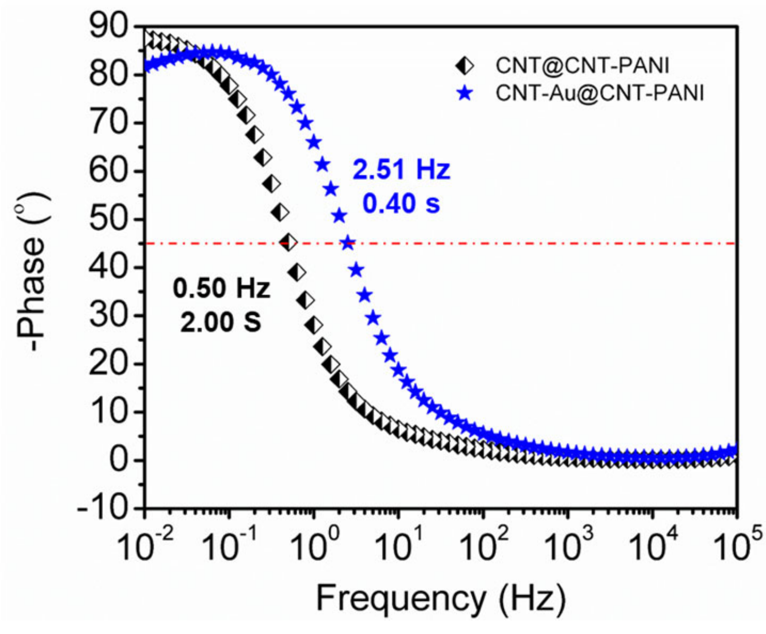

Figure S21 Dependence of impedance phase angle on frequency for CNT@CNT-PANI and CNT-Au@CNT-PANI electrodes at 0.6V versus SCE.

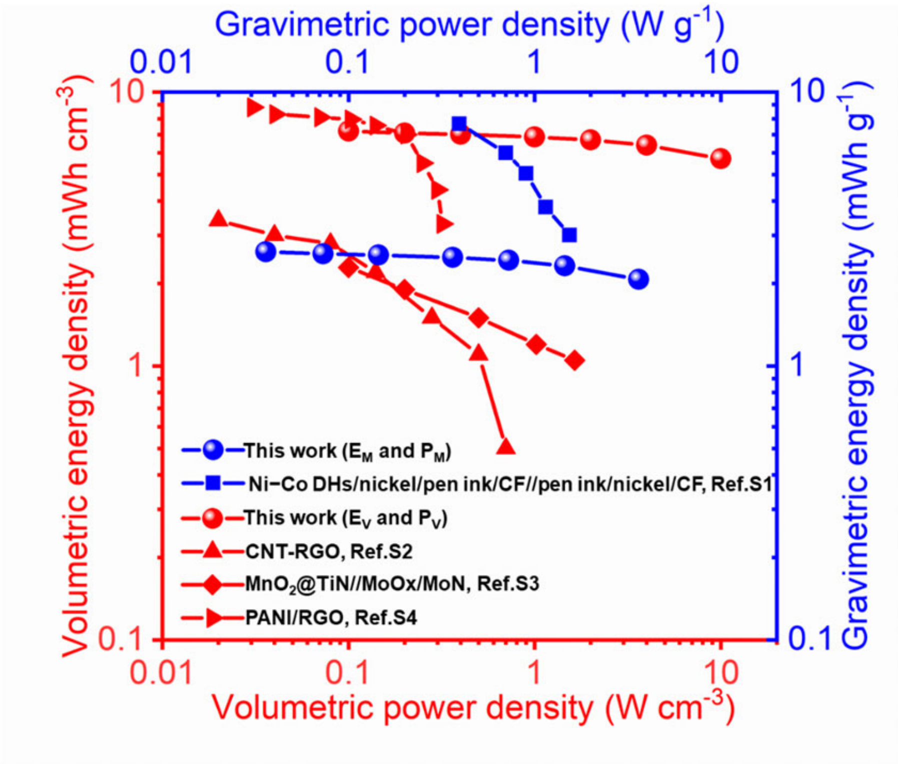

Figure S22 Ragone plots of our fiber-shaped supercapacitor based on CNT-Au@OCNT-PANI using gel electrolyte compared with previous reports[S1-S4].

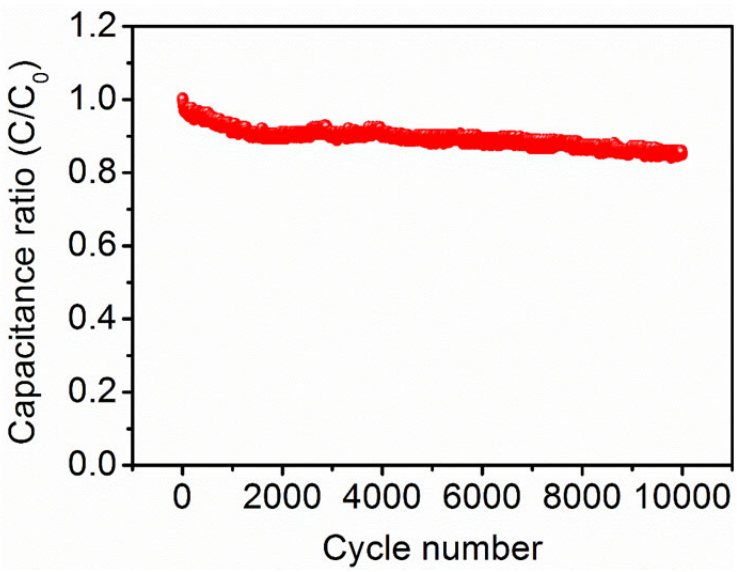

Figure S23 Cyclic stability for the fiber-shaped supercapacitor based on CNT-Au@OCNT-PANI with gel electrolyte at a current density of 10 A cm^{-3}. C_0 and C referred to the capacitances before and after cycling, respectively.

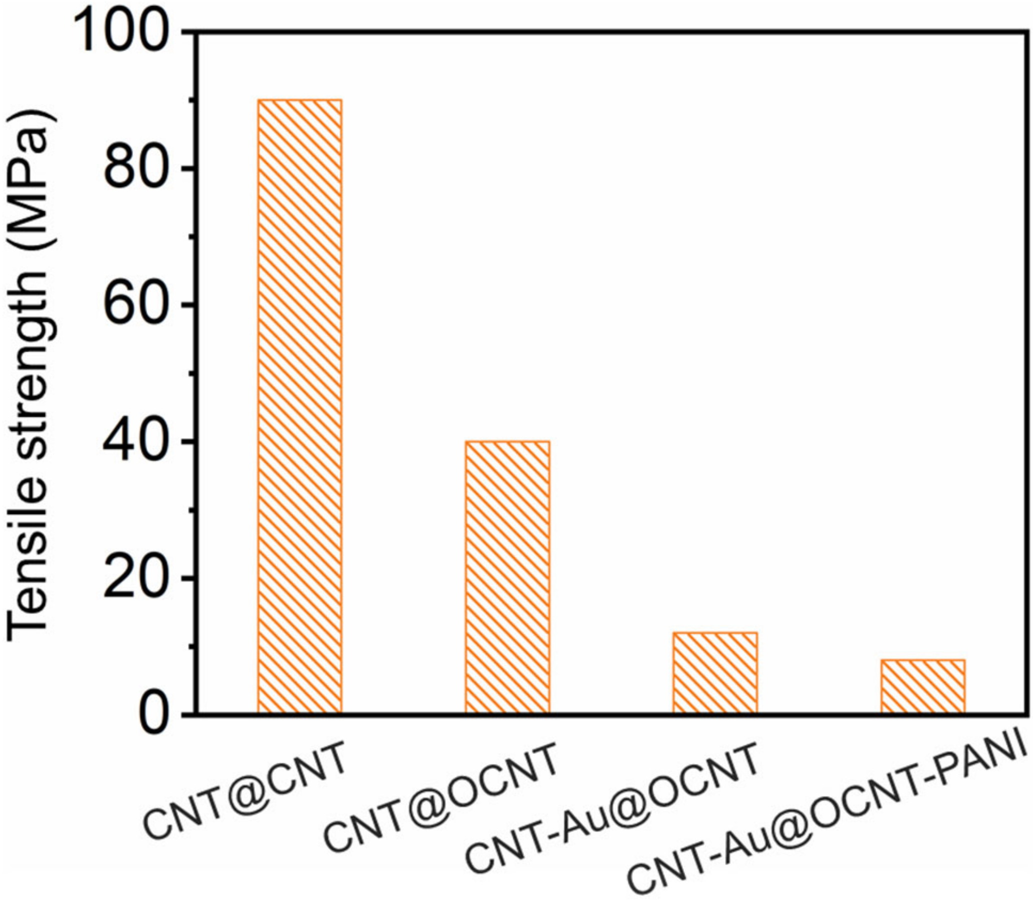

Figure S24 The tensile strengths of CNT@CNT, CNT@OCNT, CNT-Au@OCNT, CNT-Au@OCNT-PANI fibers.

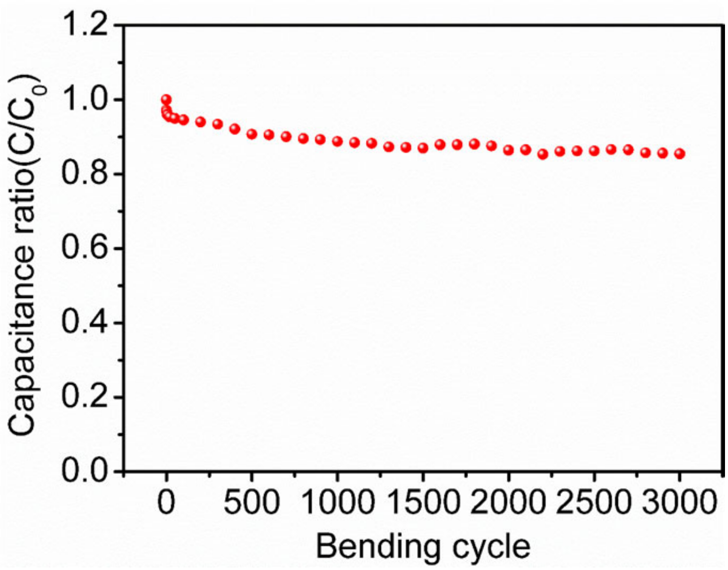

Figure S25 Dependence of capacitance retention on bending cycle at a bending angle of 90° for the fiber-shaped supercapacitor based on CNT-Au@OCNT-PANI with gel electrolyte. C_0 and C referred to the capacitances before and after bending, respectively.

References for the Supporting Information

S1 Gao L, Surjadi JU, Cao K, et al. Flexible fiber-shaped supercapacitor based on nickel−cobalt double hydroxide and pen ink electrodes on metallized carbon fiber. ACS Appl Mater Interfaces, 2017, 9: 5409-5418

S2 Ma Y, Li P, Sedloff JW, et al. Conductive graphene fibers for wire-shaped supercapacitors strengthened by unfunctionalized few-walled carbon nanotubes. ACS Nano, 2015, 9: 1352-1359

S3 Yu M, Cheng X, Zeng Y, et al. Dual-doped molybdenum trioxide nanowires: a bifunctional anode for fiber-shaped asymmetric supercapacitors and microbial fuel cells. Angew Chem Int Ed, 2016, 55: 6762-6766

S4 Li P, Jin Z, Peng L, et al. Stretchable all-gel-state fiber-shaped supercapacitors enabled by macromolecularly interconnected 3D graphene/nanostructured conductive polymer hydrogels. Adv Mater, 2018, 30: 1800124